Pertanika J. Sci. & Technol. 30 (1): 201 - 220 (2022)

PERTANIKA JOURNALS

SCIENCE & TECHNOLOGY

Journal homepage: http://www.pertanika.upm.edu.my/

Performance of a HAWT Rotor with a Modified Blade Configuration

Tabrej Khan[1], Balbir Singh[1,2], Mohamed Thariq Hameed Sultan[1,3,4] and Kamarul Arifin Ahmad[1,5]*

[1]Department of Aerospace Engineering, Faculty of Engineering, Universiti Putra Malaysia, 43400 UPM, Serdang, Selangor, Malaysia
[2]Department of Aeronautical and Automobile Engineering, Manipal Institute of Technology, Manipal Academy of Higher Education, Manipal 576104, India
[3]Laboratory of Biocomposite Laboratory, Institute of Tropical Forestry and Forest Products (INTROP), Universiti Putra Malaysia, 43400 UPM, Serdang, Selangor, Malaysia
[4]Aerospace Malaysia Innovation Centre (944751-A), Prime Minister's Department, MIGHT Partnership Hub, Jalan Impact, Cyberjaya 63000, Selangor, Malaysia
[5]Aerospace Malaysia Research Centre, Faculty of Engineering, Universiti Putra Malaysia, 43400 UPM, Serdang, Selangor, Malaysia

ABSTRACT

As the world focuses more on clean and green Earth, wind energy plays a significant role. Wind energy is a renewable source of energy that can cope with the ongoing global fossil fuel crisis. The wind energy converters like wind turbines have been studied a lot in terms of design and performance. The current work includes analyzing the output effects of a horizontal axis wind turbine (HAWT) with a modified blade configuration at specific wind speeds. A numerical investigation is carried out using two different numerical software on the chosen airfoil used in blade design validated with the analysis carried out in open-loop wind tunnels. The study is divided into two phases: first, the selected airfoil is tested experimentally and using CFD, and then the findings are compared to those of the University of Illinois Urbana Champaign wind tunnel tests at low Reynolds numbers. The second phase includes the numerical analysis based on the blade element momentum method and non-linear lifting line simulations of modified blade design at high Reynolds number. The numerical results of rotor performance analysis have been compared to existing experimental results. The findings of all numerical investigations agree with those of the experiments. An optimal value of the power coefficient is obtained at a particular tip speed ratio close to the desired value

ARTICLE INFO

Article history:
Received: 04 May 2021
Accepted: 09 August 2021
Published: 14 December 2021

DOI: https://doi.org/10.47836/pjst.30.1.11

E-mail addresses:
tabrejkhan279@gmail.com (Tabrej Khan)
balbir.s@manipal.edu (Balbir Singh)
thariq@upm.edu.my (Mohamed Thariq Hameed Sultan)
aekamarul@upm.edu.my (Kamarul Arifin Ahmad)
* Corresponding author

ISSN: 0128-7680
e-ISSN: 2231-8526

for large wind turbines. For maximum power, this study investigates the optimum pitch angle. The work demonstrated the improved HAWT rotor blade design to produce better aerodynamic lift and thus improve performance.

Keywords: Aerodynamics, computational fluid dynamics, pitch angle, turbine blade, wind energy, wind speed

INTRODUCTION

Wind energy has evolved considerably for decades and established its role as an essential substitute for developing renewable energy (Pinto et al., 2020). In tropical climates with reasonably constant wind speed, wind energy has very significant potential. A summary of various numerical studies performed in the past shows that micro-siting, modeling and estimation, rotor and turbine optimization, modeling in terms of blade and flow, and structural analysis are the highest priority fields of study (Sudhamshu et al., 2016). Figure 1 shows the wind turbine classification between the horizontal axis (HAWT) and the vertical axis (VAWT) wind turbine. There is a range of benefits of the horizontal axis wind turbine (HAWT) compared to the vertical axis wind turbine. In the case of HAWT, the rotor angle plays a significant role in rotating the turbine to generate the aerodynamic impact for the rotor coupled with the generator to produce power. Therefore, the drag force that induces reverse flow and rotor speed reduction must be reduced to enhance performance. In addition, the vortex on the blade's tip is decreased by the winglets, increasing the output by flow separation of the tip (Satwika et al., 2019). By diffusing the vortices from the blade tips,

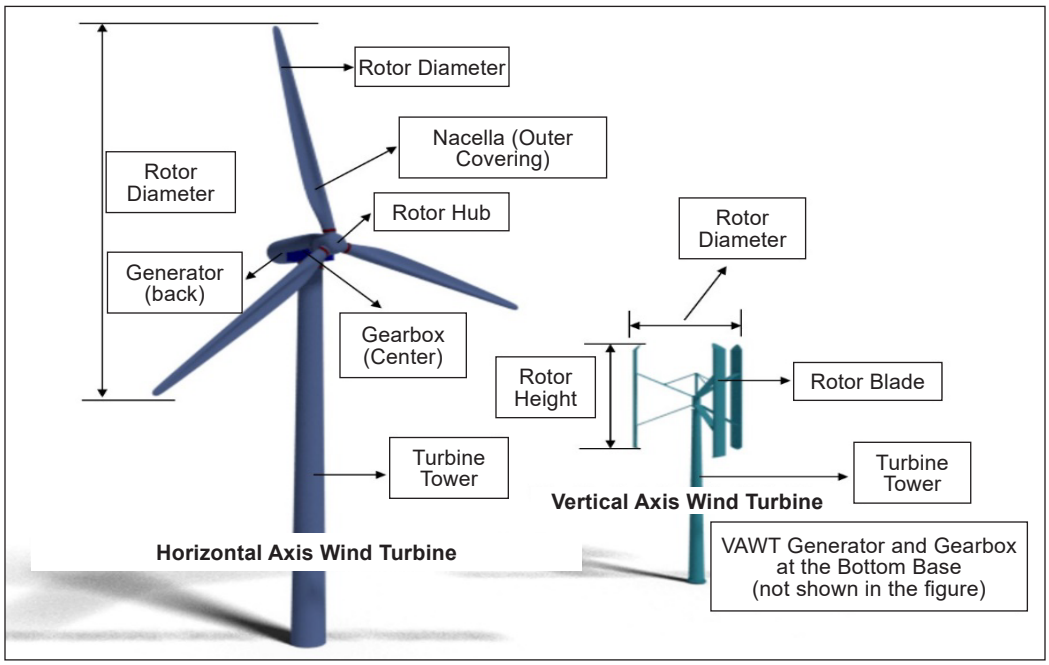

Figure 1. Typical configurations of horizontal and vertical axis turbines

winglets will reduce the impact of wingtip vortices on the turbine performance (Farhan et al., 2019).

In wind turbines, the lift force creates the rotor torque due to pressure distribution, which slotting can alter. However, this distribution change keeps the rotational velocity under control even in extreme wind speeds (Navinkumar et al., 2021). A HAWT is outstanding in energy efficiency, producing relatively constant torque and demonstrating higher power coefficients. The nacelle is hard to maintain and repair because it is heavy and accommodates the gearbox and generator. The yaw instrument rotates the nacelle completely 360 degrees to align the blade front in the wind direction (Kim & Suh, 2019). For the HAWT configuration, the aerodynamic efficiency under the yaw is very critical. With the rise in yaw angle, the wind turbine's power reduces as per cosine law (Ye et al., 2020). CFD analysis is essential for precise performance research of these blades, including flow physics.

However, Blade Element Momentum Theory is used to estimate performance compared to CFD to do it reasonably quickly (Kumar et al., 2019). The coupling between wall-resolved large eddy simulation (LES) and the blade element momentum theory (BEM) is the basis of the structure. It helps to understand the aerodynamics of the airfoil and the wind turbine and enables a wide range of turbine operating conditions to be addressed with reduced computational costs (Revaz et al., 2020). Fluid-Structure Interaction reveals that in a velocity shear state, deformation of the turbine blades enhances relative to uniform flow (Hafeez et al., 2019). FSI has been conducted many times before on wind turbines, covering various applications and interests. For instance, the k-ε-SST turbulence model uses 2D and 3D computational fluid dynamics (CFD) simulations of a vertical axis wind turbine (VAWT) (Santo et al., 2019). Most current airfoils maximize the sub-atmospheric pressure by altering the airflow from the leading edge through a slat. At elevated pressure, the air movement is from the leading edge to the trailing edge until it is pushed at the corner of the vent (Yang et al., 2020). However, aerodynamic efficiency is significantly impaired by disturbances of any kind, such as ice accretion on the blades (Jin et al., 2020).

The past research indicates that HAWT has higher performance than VAWT (Albuquerque & Matos, 2016). In this paper, a new approach is used to assess the performance of a HAWT wind turbine blade. Three different airfoils are chosen to design the turbine blade to reduce the design complexity, cost, followed by aerodynamic and performance analysis. The Clark Y airfoil used as one of the airfoils is first tested numerically and experimentally and is then used in the fabrication process. Experimental validation is performed in both airfoil and blade analysis to ensure the accuracy of the results. The numerical investigation uses blade element momentum (BEM) Theory and non-linear lifting line (LLT) algorithms to analyze the blade performance. In addition, in terms of optimal pitch angle, the efficiency of the blade and the rotor is checked. The

primary objective of this research is to analyze the performance of the new modified design of a wind turbine blade and rotor at a high Reynolds number using numerical and experimental methods.

DESCRIPTION OF PROBLEM

The performance of the HAWT turbine rotor blade is studied here. The use of low Reynolds number airfoil for 30% of the blade towards the tip is first studied numerically using computational fluid dynamics with wind speeds of 7 m/s and 14 m/s, at different angles of attack and Reynolds number. The findings are compared to the Universiti Putra Malaysia and University of Illinois Urbana Champaign open-circuit wind tunnel experimental data. The blade profile is then designed using three different airfoils, DU84132V, NACA643618, and Clark-Y, modeled based on parameters, such as increased Reynolds number, wind speed, and optimized using the profile, tip speed, and maximum lift to drag ratios. The simulations are performed in Qblade and validated with experimental data from already published work. The turbine blade profile is shown in Figure 2, with the corresponding chord lengths at each section. For the turbine, the cut-in wind speed is 3 m/s. The rotor blade is also analyzed structurally.

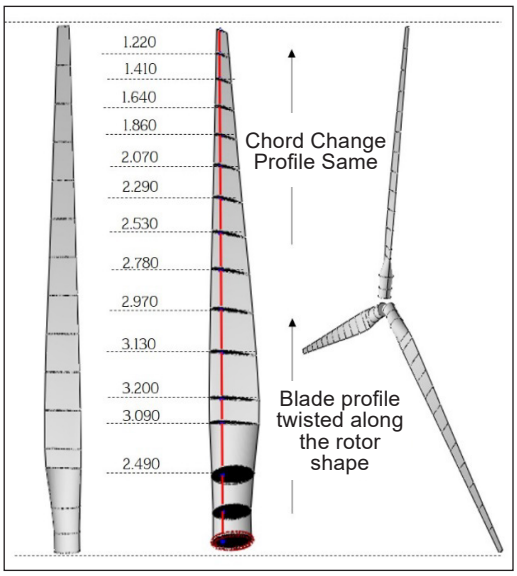

Figure 2. Blade design and section twist

BACKGROUND AND GOVERNING EQUATIONS

A traditional approach to solving a wind turbine blade design or control problem is to minimize the actual, complex configuration into a simple mechanical model that depends only on significant parameters. Then analytical, semi-analytical, and numerical methods are used (Li et al., 2014). At a high Reynolds number, the flow is turbulent across the blades. Steady Reynolds averaged continuity and momentum equations are solved at given flow conditions (Sudhamshu et al., 2016).

The sectional schematic diagram of the airfoil with the corresponding forces and angles associated with it is shown in Figure 3. As seen in the diagram, the blades rotate in the turbine's plane of rotation (POR). The twist angle β is the chord line's sectional twist angle concerning the plane of rotation. From the reference (Sudhamshu et al., 2016), for dynamic blade control, it is again helpful to use an additional twist angle called the global

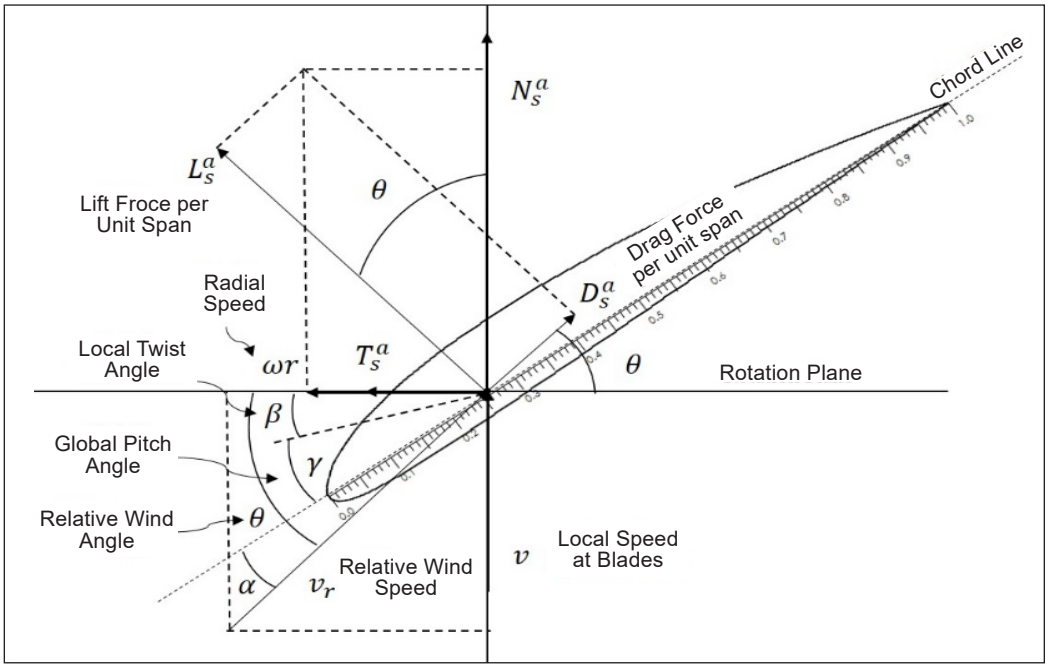

Figure 3. Forces acting on the aerofoil (Sudhamshu et al., 2016)

pitch angle ∅, which changes the twist of every cross-section by ∅. Rigid configurations of a HAWT blade and a blade section are shown in Figure 4. Due to the twisted blade profile and inclination, there is a bias '$\boldsymbol{e'}$ between the center of mass of the hub and the centroid of the blade root. This bias includes the effect of the hub radius. There is no symmetry of the blade section concerning the chord line (Li et al., 2014). The blade system is complicated in its rotation as it moves along with a huge twist towards the blade's tip, as shown in Figure 2. As shown in Figures 4 and 5, $\boldsymbol{U}_\infty$ is the oncoming wind speed, and $\boldsymbol{\omega}$ is the angular rotation, $\hat{\boldsymbol{u}}_{\boldsymbol{z}}$ into the wind, $\hat{\boldsymbol{u}}_{\boldsymbol{r}}$ along with the blade profile, and $\hat{\boldsymbol{u}}_{\boldsymbol{\theta}}$ is in the direction of rotation. Airfoil is moving in the $\hat{\boldsymbol{u}}_{\boldsymbol{\theta}}$ direction. The radial speed is $\boldsymbol{\omega r}$ where $\boldsymbol{r}$ is the distance from the center of the hub. $\boldsymbol{\omega}_\infty$ creates some force on the airfoil section. $\boldsymbol{L_s^a}$ and $\boldsymbol{D_s^a}$ are the sectional lift and drag forces, respectively, perpendicular to each other. For designing a wind turbine rotor blade, it is essential to estimate the amount of moment this force on the blade is generating. $\boldsymbol{F_\theta^a}$ and $\boldsymbol{F_z^a}$ are the forces in the $\hat{\boldsymbol{u}}_{\boldsymbol{\theta}}$ and $\hat{\boldsymbol{u}}_{\boldsymbol{z}}$ (Equations 1, 2 & 3).

$$\boldsymbol{F_\theta^a = L_s^a \cos\theta - D_s^a \sin\theta} \quad [1]$$

$$\boldsymbol{F_z^a = -L_s^a \sin\theta - D_s^a \cos\theta} \quad [2]$$

$$\boldsymbol{M = r.F_\theta^a = r.(L_s^a \cos\theta - D_s^a \sin\theta)} \quad [3]$$

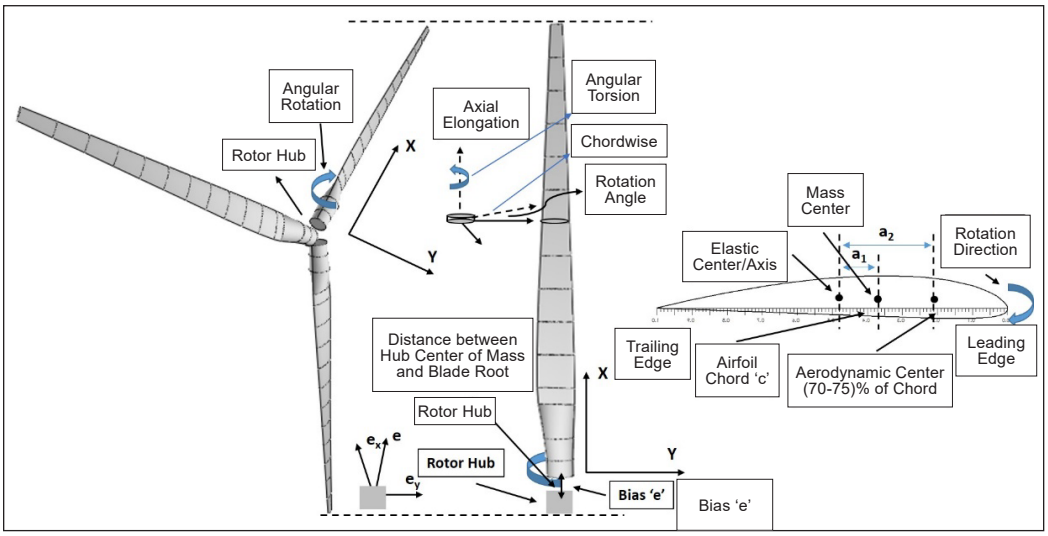

Figure 4. The detailed rigid geometry of our HAWT design

As per reference (Sudhamshu et al., 2016), the coefficient of pressure $\boldsymbol{C_P}$ can be used to quantify the pressure distribution across the airfoil in a non-dimensional way, defined as Equation 4

$$\boldsymbol{C_P} = \frac{(\boldsymbol{P} - \boldsymbol{P_\infty})}{\left[\frac{1}{2}\boldsymbol{\rho}\left(\boldsymbol{U_\infty}^2 + \boldsymbol{\omega r}^2\right)\right]} \qquad [4]$$

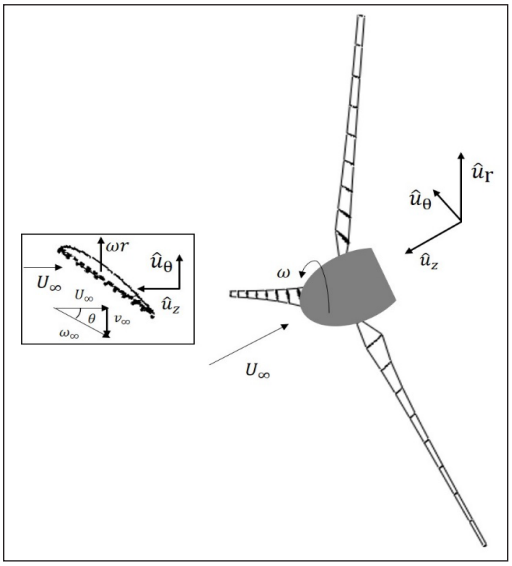

Figure 5. Rotor blade velocity profile

DETAILED METHODOLOGY

The methodology used in this study includes selecting appropriate airfoils for design and fabrication and numerical and experimental investigations to comprehend blade performance completely. Though it is standard practice in the industry to build high Reynolds number wind turbine blades with standard DU84-132V3 and NACA 64(3)-618 airfoils, or even a combination of the two, the design is complex, the fabrication process is complicated, and the turbine blade is heavy. Therefore, we strive to improve the design by incorporating a simple low Reynolds number airfoil known as the Clark Y at least 30% until the tip end. This airfoil has a high glide ratio in subsonic flow conditions. The base and the middle portion remain the combination of the standard airfoils, which reduces the design's complexity and weight to some extent.

Incorporating Clark Y airfoil in the design needs thorough investigation by adequate aerodynamic analysis using open-circuit wind tunnels, computational fluid dynamics, and structural analysis. The properties of all these selected airfoils chosen are listed in Table 1.

Qblade software was used to calculate the pressure distribution, lift and drag characteristics of the selected airfoils, as shown in Figure 6. Due to wind tunnel limitations, aerodynamic analysis was performed on Clark Y for Re value of 200k and 400k typically associated with a wind speed of 7 m/s and 14 m/s. In the aerodynamic laboratory, the Clark Y airfoil used in this experiment was fabricated. Tests were carried out in the UPM subsonic wind tunnel with an operational speed range of 0.01-0.15 Mach with stagnation pressure varying from 120 kPa to 1200 kPa. The UPM wind tunnel test section is 1 meter square with a maximum velocity of 50 m/s, illustrated in Figure 7(a). A six-component internal balance is used to measure all forces and moments. The angle blade's attack on which the lift depends is determined by the relative wind direction, the current blade length, and the line angle (Yang et al., 2020). The combination of experimental results assisted by the numerical results from computational fluid dynamics gave sufficient evidence of its fabrication and was used in the blade design. To further confirm the findings, the experimental outcomes were also compared with UIUC wind tunnel data (https://m-selig.ae.illinois.edu/uiuc_lsat.html).

The numerical investigation of Clark-Y was carried out in a Phoenics-VR environment to support the experimental part, and the airfoil was modeled using CATIA V5. As shown in Figure 7(b), C-H type mesh is always adopted for this type of study (Yan et al., 2019), but in Phoenics-VR, the grid dimension is total cell number along a single direction. As

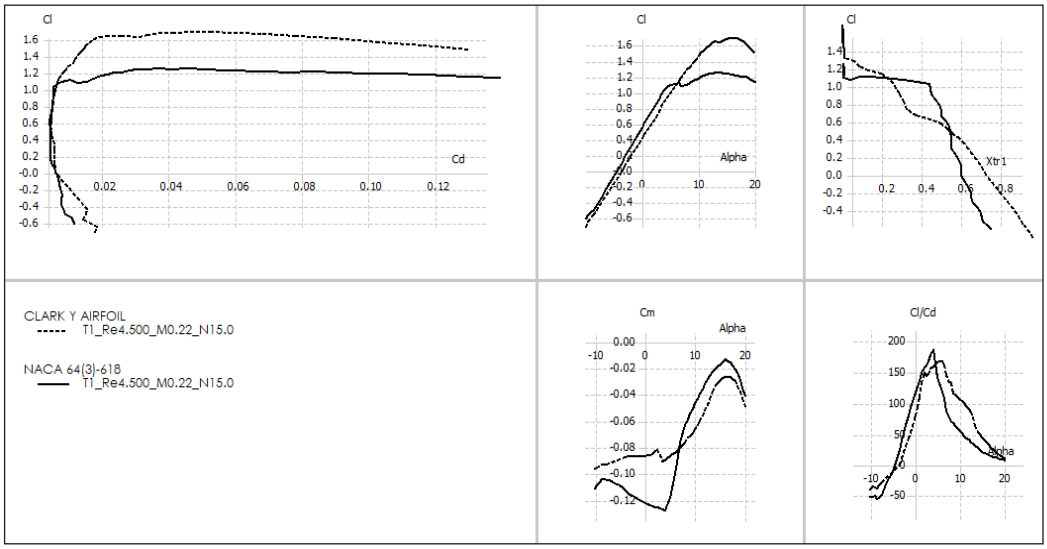

Figure 6. The performance simulations of airfoils in Qblade at M = 0.22 with Ncrit (free flow turbulence measuring parameter) of 15

shown in Figures 8(a) and 8(b), the airfoil meshed with open and closed wall domains, and flow is incompressible. The boundary outside is typically 15 chord lengths from the surface. Suitable boundary conditions were applied, and nonslip wall conditions were set up. A periodic condition is enforced in the spanwise direction as in (Yan et al., 2019). The turbulence model 'KEMODL'was used in simulation-based on 'elliptic-staggered' equation formulation. The numerical findings were then compared with the University of Illinois at Urbana-Champaign (UIUC) data considered a benchmark for such cases.

The turbine blade modified with three airfoils is then imported into the QBlade to optimize and model the large turbine blade rotor in the second phase. A complete analysis of the designed rotor was carried out in QBlade, which includes blade design and optimization with 3D visualization, rotor performance concerning tip speed ratio, turbine performance over a wind speed range, use of blade element momentum (BEM) algorithms, linear lifting line simulations, structural blade design, and analysis. Optimum pitch angle value

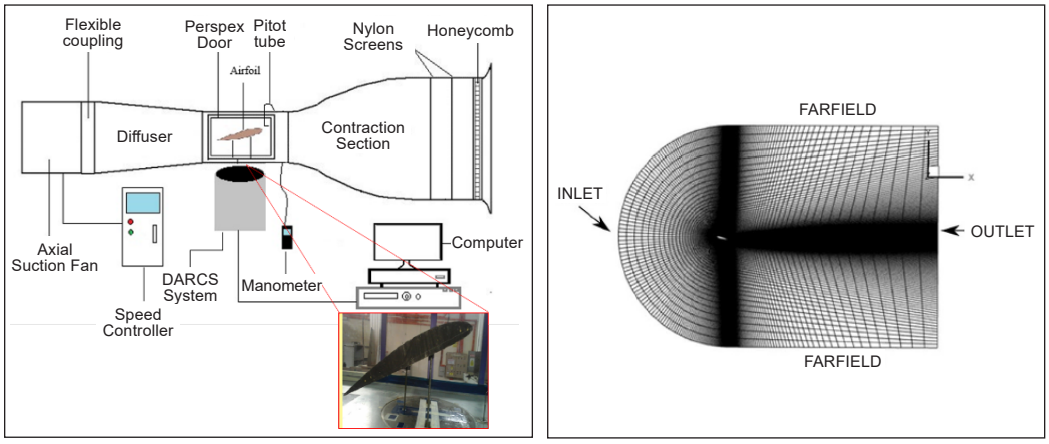

(a) (b)

Figure 7. (a) UPM wind tunnel layout and Clark Y model in the test section; (b) C-H type computational domain. Reprinted from (Yan et al., 2019), with the permission of AIP Publishing.

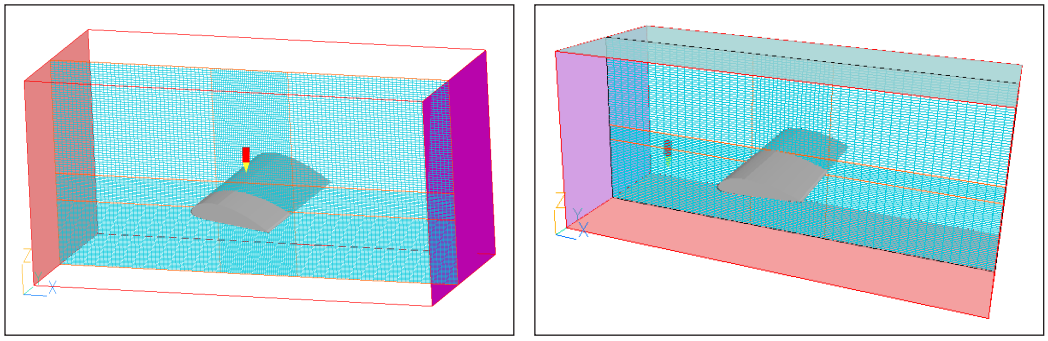

(a) (b)

Figure 8. (a) Open wall meshed domain setup; and (b) closed wall meshed domain setup

can be determined based on the lift and drag coefficient values gained from several blade segments (Satwika et al., 2019). It is important to note that the effectiveness of lift force is always more significant than the drag force increase, and also, the addition of a winglet on the tip of the turbine blade gives good performance in low tip speed ratio conditions (Satwika et al., 2019).

Table 1
Properties of the selected airfoils used in modeling

Airfoil	Chord Length	Maximum Thickness	Camber
Clark Y	28%	11%	3.4%
	42%	11%	3.4%
NACA643618	34.7%	17.9%	3.3%
	50.0%	17.9%	3.3%
DU84132V	33.9%	13.6%	3.3%
	45.3%	13.6%	3.1%

RESULTS AND DISCUSSIONS

Airfoil Analysis

The effect of velocity and pressure in the airfoil vicinity is clearly shown in pressure and velocity contours obtained from the CFD simulation. It is observed that pressure has both negative and positive values. Negative pressure means that the pressure is lower than the ambient pressure and vice versa. In Figure 9(a), for velocity 7 m/s at a -4 degrees angle of attack, the highest pressure region is found at the upper surface's leading edge. It is also the location of the stagnation point where the local velocity of the fluid ceases. Therefore, the negative pressure region on the airfoil's upper surface is more significant than that on the lower surface.

This change in pressure distribution causes lifts to increase. The maximum pressure at the leading edge is 33.15187 Pa, while the minimum pressure at the trailing edge is 16.24748 Pa, which gives a pressure drag of 16.90439 Pa. The variation in pressure drag depends on the maximum and minimum pressures at leading and trailing edges. The average pressure around the airfoil is between 0 Pa and 3 Pa. Referring to Figure 9(b), for velocity 7 m/s at -4 degrees angle of attack, it is observed that the highest velocity is 8.890738 m/s at the middle of the upper surface and the vicinity of the leading edge of the lower surface. Therefore, in the region of minimum pressure, the velocity is maximum.

The trailing edge velocity is found in the range of 3 to 5, which is still less than the values on the upper and lower surfaces of the airfoil. For velocity 7 m/s at the trim angle of attack, the more significant negative pressure suction at the upper surface can be observed than at the lower surface. The highest pressure is 32.65910 Pa at the leading-edge stagnation point. The velocity contour also shows that velocities of around 4 m/s are found at the

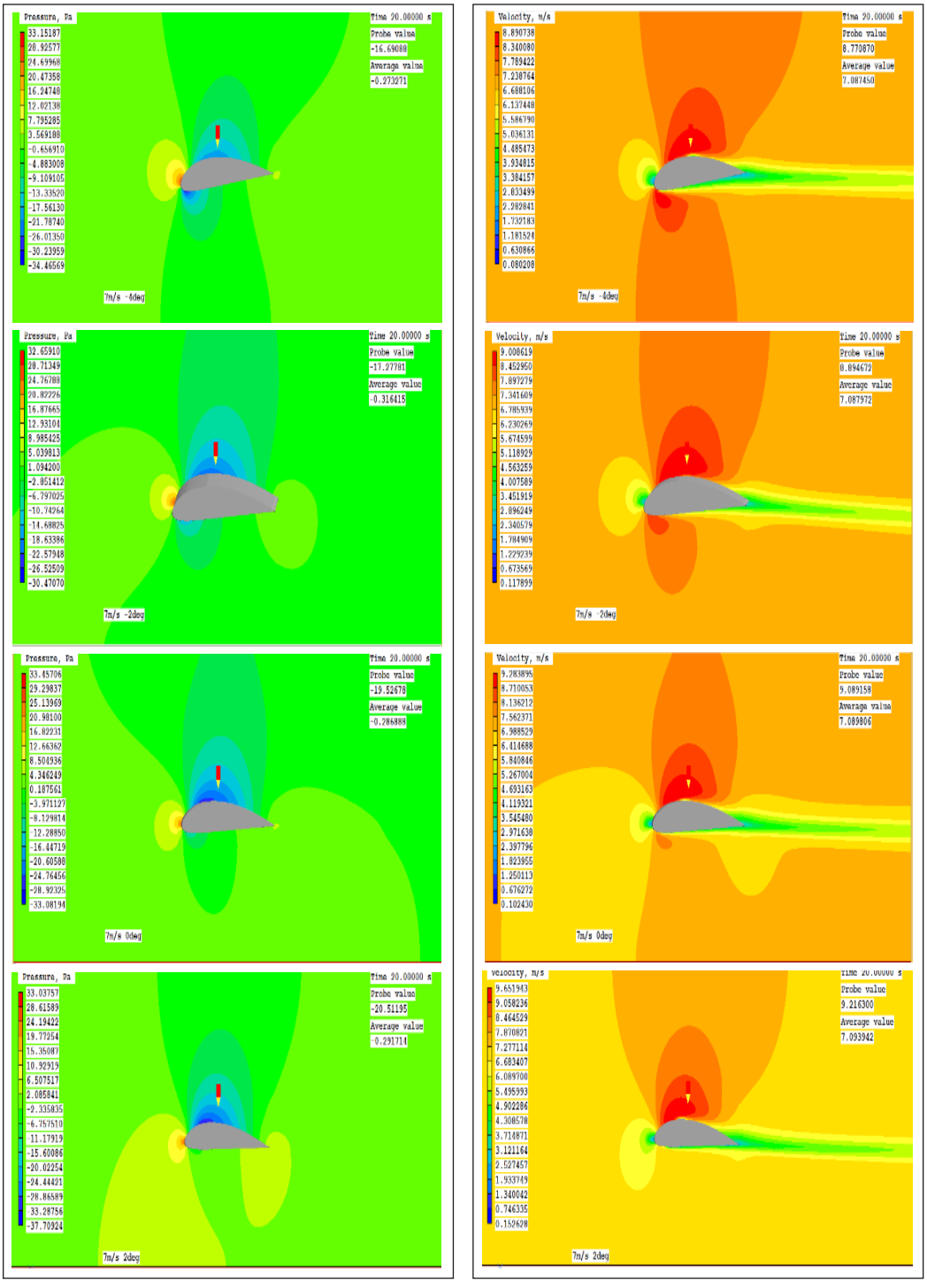

(a) (b)

Figure 9. Clark Y airfoil (a) Pressure and (b) Velocity Contours for 7 m/s at -4, -2, 0 and 2 degrees AOA

leading and the trailing edges. The airfoil's upper surface is the highest velocity region with a velocity over 9 m/s due to the lowest pressure gradient. Contours also show the wake production at the back of the airfoil.

For velocity 7 m/s at 2 degrees angle of attack, as the angle of attack increases, the pressure on the upper surface is more significant than that on the lower surface. The pressure suction on the lower surface is smaller than the -4 and -2 degrees angle of attack. The lowest pressure is -33.08194 Pa, whereas most of the pressure in the domain is around 4.346249 Pa. The highest velocity is 9.283895 m/s, and it is found in the upper region of the airfoil.

A velocity value of around 4 m/s is found at both the leading and trailing edges. Referring to Figure 10(a), the lower pressure region under the airfoil disappeared for a velocity of 14 m/s at a -4 degrees angle of attack. The negative pressure suction can be seen only on the upper surface. Two moderate pressure values are observed in front of the airfoil and behind it. The pressure difference becomes high, and so does the pressure drag. The corresponding velocity values are found in the airfoil's upper region, with higher velocity gradients. The difference in velocities on the top and bottom of the airfoil becomes large. When the angle of attack is higher, we can see that the streamlines above the airfoil become denser than those under the airfoil. For velocity 14 m/s at a -2 degrees angle of attack, it can be observed that there is more significant negative pressure suction at the upper surface than that at the lower surface. The highest pressure is 129.8730 Pa occurring at the leading-edge stagnation point. Referring to Figure 10(b), the velocity contour at a -2 degree angle of the attack shows that velocities of around 9 m/s are found at the leading and the trailing edge. The highest velocity is 18 m/s, and it is found in the region of the lowest pressure gradient. For velocity 14 m/s at trim degrees angle of attack, the pressure on the upper surface is more significant than on the lower surface. The lowest pressure is around -88 Pa, whereas most of the domain's pressure is around -14 Pa. The highest velocity is 18.70307 m/s at the upper region of the airfoil.

Validation of Airfoil Results

Referring to Figures 11(a) and 11(b), at Reynolds number 2×10^5, the CFD results are in good agreement with the experimental data obtained from wind tunnels; the higher the alpha, the larger the lift coefficient. Subsequently, the slopes are almost linear. The data-related lift coefficients obtained from the experiments in the UPM wind tunnel are lower than the values of the UIUC wind tunnel experiment and CFD data with relevancy at angles of attack of -4 to 0 degrees. The lift coefficients of CFD analysis are slightly larger than those of UIUC wind tunnel data. The maximum lift coefficient for UIUC wind tunnel data is 1.309 at an AoA of 12.35 degrees, while that of UPM wind tunnel data is 0.743 at an AoA of 13 degrees.

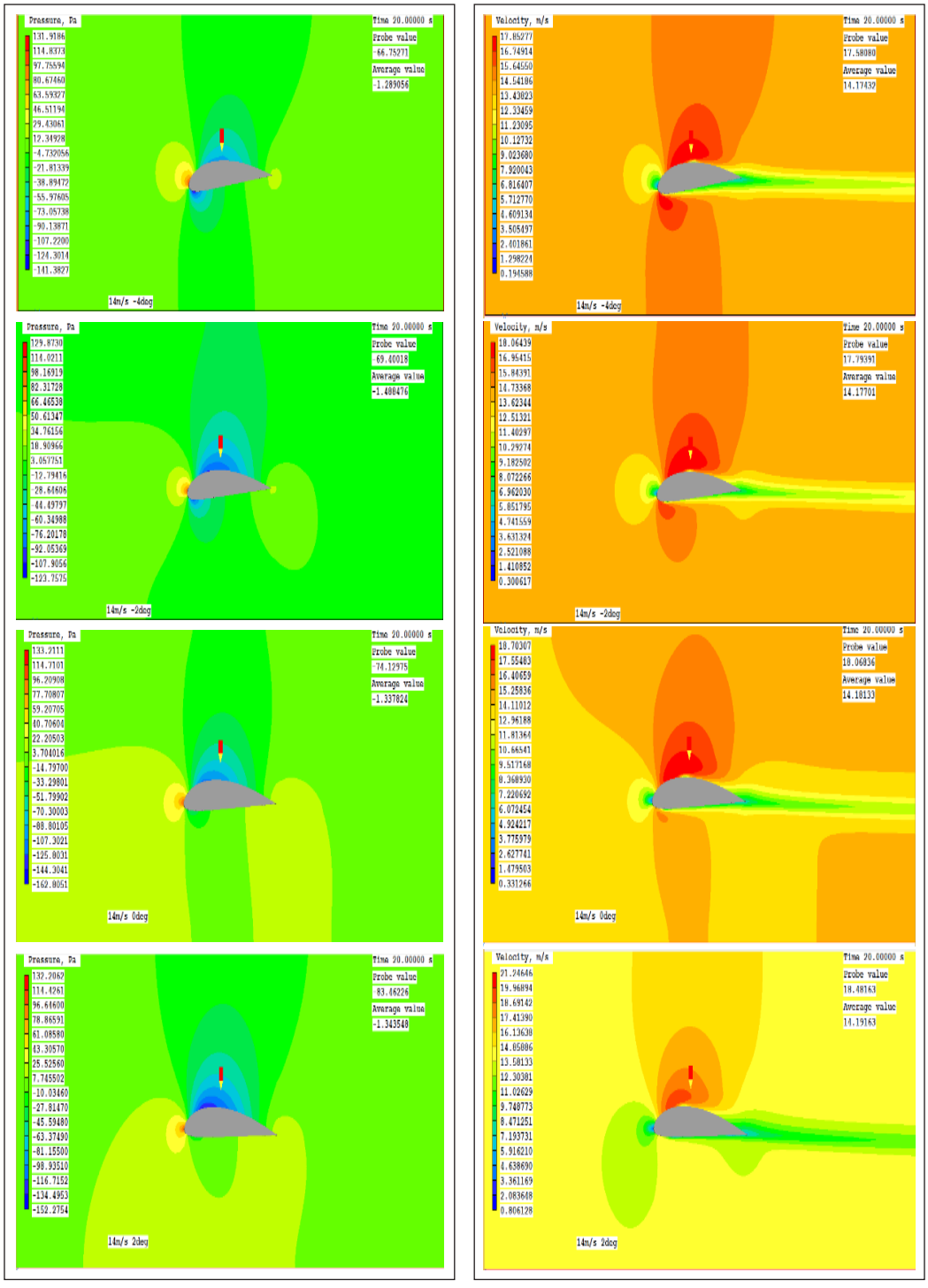

(a) (b)

Figure 10. Clark Y airfoil (a) Pressure and (b) Velocity Contours for 14 m/s at -4, -2, 0 and 2 degrees AOA

The CFD analysis gives a maximum lift coefficient of 1.456 at an AoA of 14 degrees. The maximum drag coefficient occurs at AoA of 12.35 degrees, and the value is 0.0225 for the UIUC wind tunnel data. From Figures 11(c) and 11(d), at Reynolds number 399,900, both lift and drag coefficients increase. The maximum lift coefficient is 1.332 at AoA of 12.35 degrees from UIUC wind tunnel data. Thus, for the Coefficient of Drag C_D versus AoA, all the results from CFD, UIUC, and UPM wind tunnels are in good agreement with each other. The modest discrepancy in lift coefficient between the UPM and UIUC wind tunnels is due to changes in wind tunnel flow quality, measurement methods, model accuracy (i.e., significant uncertainties of parameters and model geometry during the experiment, between all three measurements. This error is also caused by a model mounting limitation, where the brace used to modify the angle of attack passes through the airfoil model, preventing the whole lift force experienced by the airfoil from being appropriately communicated to the transducer. Though this problem is wholly rectified now, this also explains the minimum error from -6 to 0 degrees angle of attack.

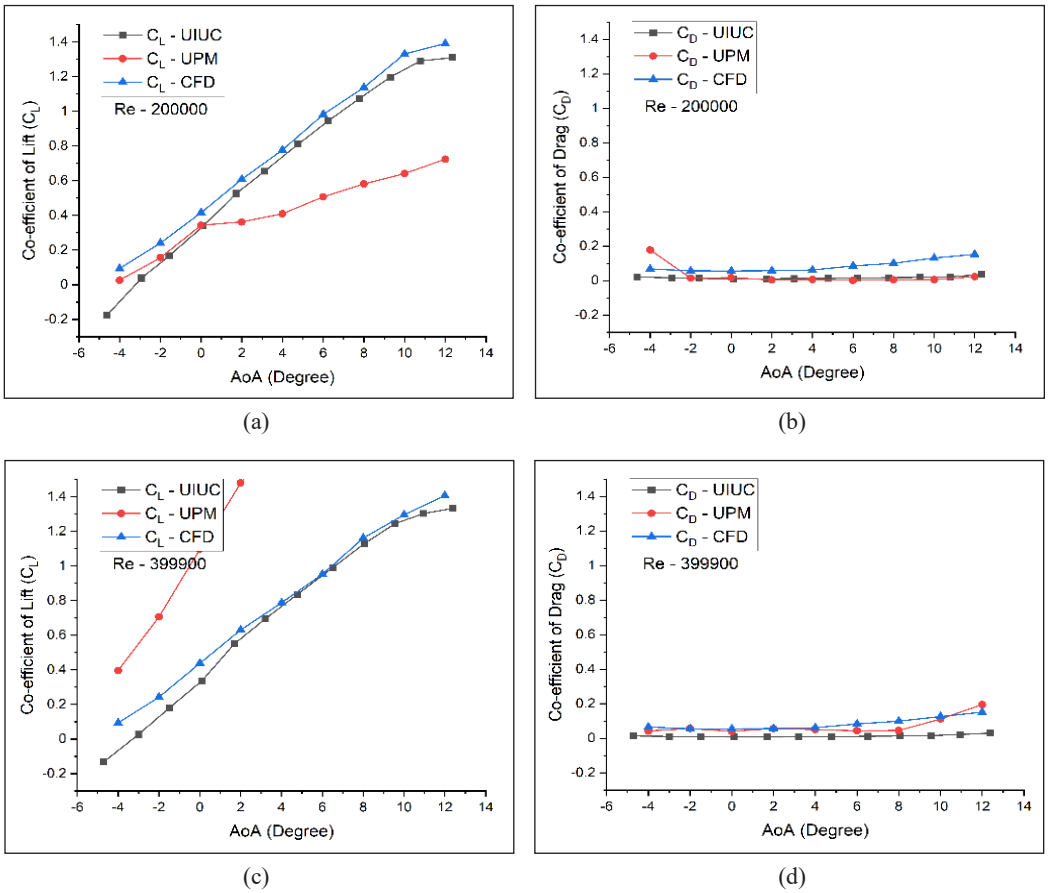

Figure 11. Numerical and experimental comparisons (a) – (b) Coefficients of lift and drag versus AoA at Re = 200000 (c) – (d) Coefficients of lift and drag versus AoA at Re = 399900

Turbine Rotor Analysis

QBlade is used to design the blade using the selected airfoils listed in Table 1 and the rotor with three blades. The blade geometry optimization was completed in the optimization module. Optimization based on the tip-speed ratio is used in this analysis, rather than the lift-to-drag ratio, which sets the corresponding twist at a specific tip-speed ratio. Therefore, it is necessary to investigate the section solidity that depends on the section chord and should be between 0 and 1 when designing the blade. The Blade Element Momentum algorithm will not converge if any segment solidity increases beyond this range of values. The blade design parameters are given below in Table 2. Computational simulations, using fluid dynamic equations and algorithms, have been widely used to predict, overcome and analyze problems involving fluid flows (Akansu et al., 2017). The blade element momentum theory combined with the lifting line method with guaranteed convergence in QBlade was used for the blade study. The airfoil coordinates were entered into the structural analysis as part of the profile (Barrett & Ning, 2016).

The structural part also takes input from Blade Element Momentum/Lifting Line Theory Analysis.

Table 2
Wind turbine rotor blade design parameters

Blade Parameter	Value
Rated Power	1.5 – 2.5 MW
No. of Blades	3 blades, upwind
Transmission	Single
Blade radius (m)	42.20
Hub Radius (m)	1
Maximum speed (rpm)	15
Cut-in wind speed (m/s)	3
Cut-out wind speed (m/s)	25
Hub Height (m)	100
Rotor Overhang (m)	7.03

Rotor BEM and Non-linear Lifting Line Analysis. A significant advantage of the Lifting Line Theory over the Blade Element Momentum approach is that it is possible to obtain velocity distribution in the flow field around the rotor. In addition, as shown in Figure 12, integrated velocity planes make it possible to access the 3D velocity field information in general.

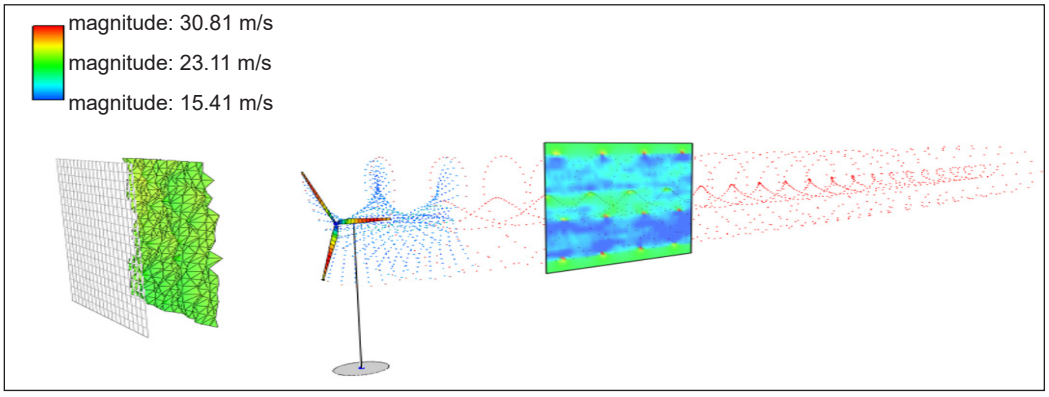

Figure 12. Velocity distribution in the rotor (side view)

A finite number of blade components are discretized into the blade. Two parts connect an element that sweeps the rotor plane on a circular track. The radial location, profile, chord, twist, and length of the blade cross-sections characterize them. It is possible to compute the relative wind speed for every section using momentum theory. Next, the normal and tangential components are calculated with these coefficients and the area of an element, thereby calculating an element's thrust and torque.

The inputs of the various components can then be applied together to obtain the total rotor thrust and torque. For different wind speeds and angular speed ratios, characteristic curves can be helpful. It is important to note that BEM looks at two crucial iteration factors related to the respective blade design for understanding. The relative wind angle θ and power of the rotor σ depends on the chord and N number of the blade (Equation 5).

$$\boldsymbol{\sigma = \frac{CN}{2\pi r}} \quad [5]$$

The relative wind angle depicts the angle of attack, the angle between the chord line, and the relative wind speed experienced by the rotor blade (Equation 6). Figure 13 shows the power in megawatts with the wind speed for the current rotor blade. The optimal rated power is close to 2 MW.

$$\boldsymbol{\alpha = \theta - (\beta + \gamma)} \quad [6]$$

Qblade also can examine blades using lifting line algorithms. As a result, it has an advantage in vortex core modeling, computational efficiency criteria, multi-threading, and wake connectivity monitoring.

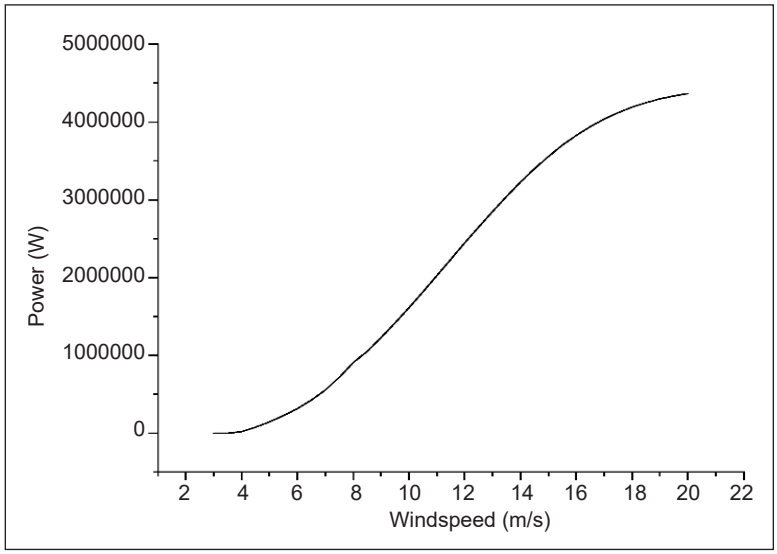

Figure 13. Power versus wind speed for the current analysis

Structural Blade Design and Analysis. The Horizontal-Axis Wind Turbine (HAWT) has a rotor with a radius of 42.2 meters and starts at the root tending with a cylindrical shape and progressing to the body and tip using Clark-Y. As a function of the radius, this wind blade often has a pitch to differ, giving it a twist and pitch angle at the blade's tip. As a result, the strength of the e-glass used on the outer shell determines the blade's maximum stress. At 15 m/s, a typically rated wind speed for a turbine at this scale, the turbulent wind flows towards the negative z-direction. It is believed that this incoming flow makes the blade rotate around the z-axis.

Therefore, the optimal tip velocity ratio equals 8, a good value for a giant wind turbine and the TSR point at which the power coefficient is maximum.

The GFRP E-Glass, widely used in wind turbine blades, is the material chosen for the other shell construction, and the inner structure is Polymethacrylimide foam (PMI). The material characteristics of each of these are given in Table 3. From the BEM/LLT studies conducted before, QBlade takes each part of the blade's load values. The blade root is offset by 1.2 meters from the rotation axis. A method for calculating average loads on a wind turbine is given in this study.

Nevertheless, the BEM theory presented several significant steady-state and dynamic effects that trigger increased loads or reduced power output, significantly increased transient loads. In Figure 14, the structural load analysis is shown.

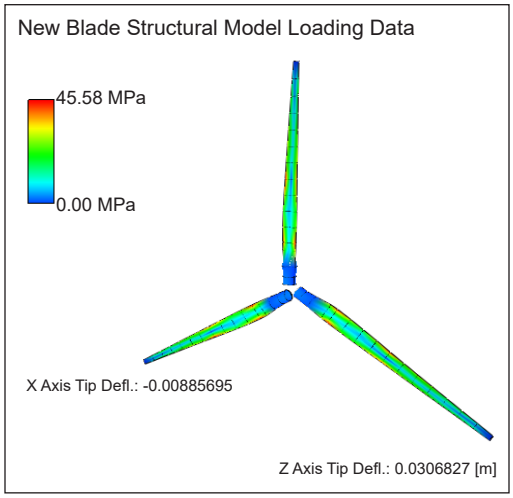

Figure 14. Structural blade modal and deflection analysis

Table 3
Blade element material properties

Blade Element	Material	Young's Modulus (GPa)	Density (kg/m^3)
Blade outer shell	GFRP (E-Glass)	7.2	2580
Blade inner Shell	PMI Foam	0.03 – 0.39	30 - 300

Validation of Results. Without validation, the second step of blade design and rotor output analysis cannot be considered successful. Wang et al. (2011) used the same blade configuration (but different airfoils) with rotor diameter and power almost identical to the current study; this was taken as a validation benchmark. For their designed rotor and turbine, Wang et al. (2011) used experimental, CFD, and FVM studies. For the full-scale 3-bladed NH1500 wind turbine, the measurement of both CFD and FVM was performed.

Figure 15 shows their comparison of the power coefficient CP with tip-speed ratio (TSR) variance based on experimental performance, CFD measurements, and FVM estimation.

The CP versus TSR results from the current study show a reasonably good agreement with Wang et al. (2011) in Figure 16. The overall CP was obtained at an optimal TSR of around 9.5, compared to 8.0 in the current study. The mean CP for the experiment was 0.492, 0.505 for the CFD calculation, 0.528 for the FVM calculation, and 0.525 for the current analysis. The higher maximum CP of both the reference and current research is very similar to the well-known limit of Betz 0.593. The maximum outcome of 0.525 from the study can therefore be persuasive.

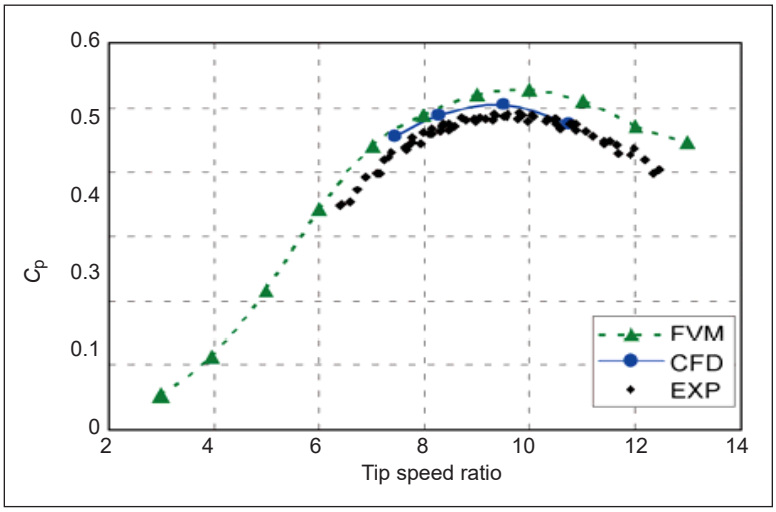

Figure 15. Relation of CP with TSR (Wang et al., 2011)

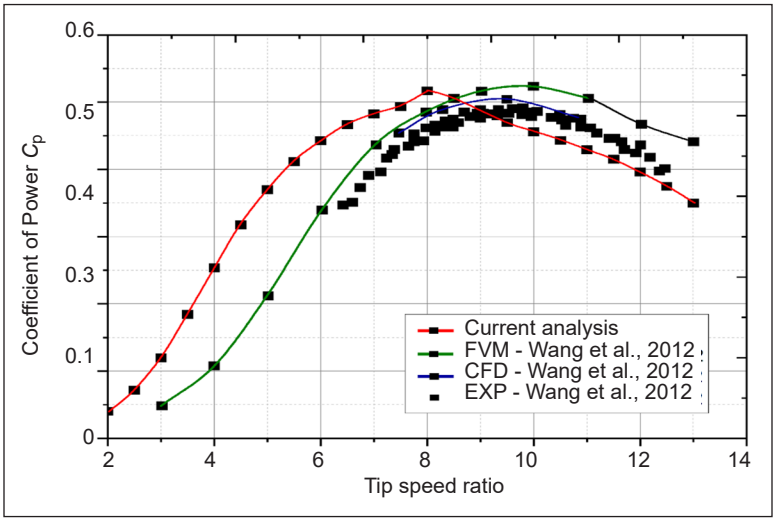

Figure 16. CP versus TSR for experimental validation (Wang et al., 2011)

CONCLUSION

This study designed and checked the performance and brief structural analyses of the Horizontal-Axis Wind Turbine (HAWT) rotor blade. The goal of studying large wind turbine blades at a high Reynolds number with a modified blade design made from three airfoils was fulfilled. Although this is a preliminary study, the outcomes are satisfactory, but it requires more extensive experimentation in the future. The first part of the paper focused on the wind turbine geometry modeling, including the airfoil selection and performance numerically and experimentally using open-circuit wind tunnels. The second part looked at the modified blade design, optimization, and performance analysis based on Blade Element Moment Theory and Lifting Line Theory using Qblade and later on validation with the experimental results. Aerodynamic equations based on selected parameters and the efficiency of selected airfoils determine a practical blade shape, according to the current study on blade design. Aesthetics has a small part to play.

The most efficient shape is made up of airfoil parts that increase in width, thickness and twist angle as they approach the hub. The paper demonstrated that the chosen 1.5–2.5 MW turbine with a diameter of more than 80 m and a hub height of 100 m has an optimal power coefficient of 0.525 at a tip speed ratio of 8, which is an excellent value for large wind turbines with this modified design. Aeroelastic uncertainty is always associated with large and flexible wind turbine blades that need thorough analysis and could be valuable to future study. The displacement of the blade tip at the nominal wind speed reduces the turbine's rated power. In the future, it is observed that the use of intensive computational BEM/LLT, fluid-structure interaction, and CFD studies with experimental analysis for new designs will help to analyze the giant wind turbine performance in detail.

ACKNOWLEDGEMENTS

The authors gratefully acknowledge the contributions of FAAS ENGINEERING AND CONSULTANCY SDN. BHD in providing opportunities to flourish and make engineering and energy-related research a reality through grant no: 6300248. The authors would also like to convey their gratitude to UPM for providing the necessary facilities required for this research work.

REFERENCES

Akansu, S. O., Dagdevir, T., & Kahraman, N. (2017). Numerical investigation of the effect of blade airfoils on a vertical axis wind turbine. *Isi Bilimi Ve Teknigi Dergisi/ Journal of Thermal Science and Technology, 37*(1), 115-125.

Albuquerque, I., & Matos, F. (2016). A characterization of vertical axis wind turbines. *IEEE Latin America Transactions, 14*(10), 4255-4260. https://doi.org/10.1109/tla.2016.7786302

Barrett, R., & Ning, A. (2016). Comparison of airfoil precomputational analysis methods for optimization of wind turbine blades. *IEEE Transactions on Sustainable Energy, 7*(3), 1081-1088. https://doi.org/10.1109/tste.2016.2522381

Farhan, A., Hassanpour, A., Burns, A., & Motlagh, Y. G. (2019). Numerical study of effect of winglet planform and airfoil on a horizontal axis wind turbine performance. *Renewable Energy, 131*, 1255-1273. https://doi.org/10.1016/j.renene.2018.08.017

Hafeez, N., Badshah, S., Badshah, M., & Khalil, S. J. (2019). Effect of velocity shear on the performance and structural response of a small-scale horizontal axis tidal turbine. *Marine Systems & Ocean Technology, 14*(2-3), 51-58. https://doi.org/10.1007/s40868-019-00057-0

Jin, J. Y., Virk, M. S., Hu, Q., & Jiang, X. (2020). Study of ice accretion on horizontal axis wind turbine blade using 2D and 3D numerical approach. *IEEE Access, 8*, 166236-166245. https://doi.org/10.1109/access.2020.3022458

Kim, S. H., & Suh, K. (2019). Experimental and numerical investigation on power characteristics of 300 W class horizontal axis wind turbine with wave winding type AFPM generator. *International Journal of Precision Engineering and Manufacturing-Green Technology, 7*(4), 837-848. https://doi.org/10.1007/s40684-019-00160-y

Kumar, P. M., Seo, J., Seok, W., Rhee, S. H., & Samad, A. (2019). Multi-fidelity optimization of blade thickness parameters for a horizontal axis tidal stream turbine. *Renewable Energy, 135*, 277-287. https://doi.org/10.1016/j.renene.2018.12.023

Li, L., Li, Y., Liu, Q., & Lv, H. (2014). A mathematical model for horizontal axis wind turbine blades. *Applied Mathematical Modelling, 38*(11-12), 2695-2715. https://doi.org/10.1016/j.apm.2013.10.068

Navinkumar, B., Parammasivam, K., Rajendran, S., & Mohanavel, V. (2021). CFD analysis of horizontal axis wind turbine braking system using chordwise spacing. *Materials Today: Proceedings, 37*, 542-552. https://doi.org/10.1016/j.matpr.2020.05.564

Pinto, M. L., Franzini, G. R., & Simos, A. N. (2020). A CFD analysis of NREL's 5MW wind turbine in full and model scales. *Journal of Ocean Engineering and Marine Energy, 6*(2), 211-220. https://doi.org/10.1007/s40722-020-00162-y

Revaz, T., Lin, M., & Porté-Agel, F. (2020). Numerical framework for aerodynamic characterization of wind turbine airfoils: Application to miniature wind turbine WiRE-01. *Energies, 13*(21), Article 5612. https://doi.org/10.3390/en13215612

Santo, G., Peeters, M., Van Paepegem, W., & Degroote, J. (2019). Dynamic load and stress analysis of a large horizontal axis wind turbine using full scale fluid-structure interaction simulation. *Renewable Energy, 140*, 212-226. https://doi.org/10.1016/j.renene.2019.03.053

Satwika, N. A., Hantoro, R., Sarwono, S., & Nugroho, G. (2019). The experimental investigation and numerical analysis on horizontal axis wind turbine with winglet and pitch variations. *Engineering Journal, 23*(6), 345-360. https://doi.org/10.4186/ej.2019.23.6.345

Sudhamshu, A. R., Pandey, M. C., Sunil, N., Satish, N. S., Mugundhan, V., & Velamati, R. K. (2016). Numerical study of effect of pitch angle on performance characteristics of a HAWT. *Engineering Science and Technology, an International Journal, 19*(1), 632-641. https://doi.org/10.1016/j.jestch.2015.09.010

Wang, T., Wang, L., Zhong, W., Xu, B., & Chen, L. (2011). Large-scale wind turbine blade design and aerodynamic analysis. *Chinese Science Bulletin, 57*(5), 466-472. https://doi.org/10.1007/s11434-011-4856-6

Yan, Y., Avital, E., Williams, J., & Cui, J. (2019). CFD analysis for the performance of micro-vortex generator on aerofoil and vertical axis turbine. *Journal of Renewable and Sustainable Energy, 11*(4), Article 043302. https://doi.org/10.1063/1.5110422

Yang, Y. K., Kim, M. Y., Song, Y. W., Choi, S. H., & Park, J. C. (2020). Windcatcher louvers to improve ventilation efficiency. *Energies, 13*(17), Article 4459. https://doi.org/10.3390/en13174459

Ye, Z., Wang, X., Chen, Z., & Wang, L. (2020). Unsteady aerodynamic characteristics of a horizontal wind turbine under yaw and dynamic yawing. *Acta Mechanica Sinica, 36*(2), 320-338. https://doi.org/10.1007/s10409-020-00947-2